Physica B 404 (2009) 2166–2171

Contents lists available at ScienceDirect

Physica B

journal homepage: www.elsevier.com/locate/physb

On the observation of a huge lattice contraction and crystal habit modifications in $LiMn_2O_4$ prepared by a fuel assisted solution combustion

K. Ragavendran *, D. Sherwood, D. Vasudevan, Bosco Emmanuel

Central Electrochemical Research Institute, Karaikudi 630 006, Tamilnadu, India

ARTICLE INFO

Article history:
Received 11 November 2008
Received in revised form
3 March 2009
Accepted 6 April 2009

PACS:
82.47.Aa
61.50.Ks
91.35.−x

Keywords:
Mixed valence
Lithium manganate
Lattice contraction
Crystal shape algorithm
Crystal habit
Poly vinyl alcohol
Geo physics

ABSTRACT

Two batches of poly-crystalline lithium manganate were prepared by a fuel assisted solution combustion method. $LiMn_2O_4$(S) was prepared using starch as the fuel and $LiMn_2O_4$(P) was prepared using poly vinyl alcohol (PVA) as the fuel. XRD studies indicated a significant and consistent shift in the 2θ values of all the *hkl* peaks to higher values in $LiMn_2O_4$(P) compared to $LiMn_2O_4$(S) indicating a lattice contraction in the former. TG/DTA studies indicated a higher formation temperature (~25 °C higher) for $LiMn_2O_4$(P). The higher formation temperature most likely promotes the oxidation of some Mn^{3+} to Mn^{4+} with a lower ionic radius causing a lattice contraction. This hypothesis is confirmed through XPS studies which indicated the presence of a higher fraction of Mn^{4+} in $LiMn_2O_4$(P) than that present in $LiMn_2O_4$(S). A crystal shape algorithm was used to generate the crystal habits of lithium manganate from their XRD data leading to an understanding on the exposed *hkl* planes in these materials. From the atomic arrangement on the exposed *hkl* planes it is predicted that $LiMn_2O_4$(P) would be less prone to manganese dissolution and hence would possess a higher cycle life when compared to $LiMn_2O_4$(S).

1. Introduction

Besides its application in the battery industry as a cost effective, environmental friendly cathode material with better safety aspects compared to $LiCoO_2$ [1–3], spinel type lithium manganate, a mixed valent compound [4,5] with Mn present in two different oxidation states viz. Mn^{3+} and Mn^{4+}, also serves as a prototype compound in the hands of a condensed matter physicist. Its application in the study of charge ordering, frustrated magnetism and geo-physics are well documented in the literature [6–8]. Physicochemical properties of such mixed valent compounds, be it of interest to an electro-chemist or a condensed matter physicist, largely depends upon the nature of the redox couple (i.e. the ratio of the mixed valent states). For instance, the Mn^{+3}–O–Mn^{+4} interaction in a perovskite manganite give rise to a double exchange ferromagnetic interaction while the Mn^{+3}–O–Mn^{+3} and Mn^{+4}–O–Mn^{+4} give rise to a super exchange anti-ferromagnetic interaction [9–11]. In the case of spinel type lithium manganate, the spin frustrated magnetism [12] and electrochemical properties [13] are determined by the nature of the Mn^{+3}/Mn^{+4} couple.

The present paper reports the interesting results observed during the characterization of $LiMn_2O_4$ prepared through solution combustion [14,15]. We observe a huge lattice contraction in $LiMn_2O_4$ when PVA is used instead of starch as the fuel. Thermo-gravimetric studies and XPS studies have been carried out and compared with that of $LiMn_2O_4$ prepared using starch as the fuel. It is found that the method of preparation alters the Mn^{3+}/Mn^{4+} ratio in $LiMn_2O_4$ which causes a lattice contraction. Crystal habits of the materials which dictate the electrochemical properties are studied using a crystal shape algorithm [16].

2. Experimental and computational part

Polycrystalline lithium manganate, $LiMn_2O_4$(S) and $LiMn_2O_4$(P) were prepared by a fuel assisted solution combustion route using starch and PVA, respectively, as the fuels. The preparation details are the same as that reported earlier [14,15]. The precursors were calcined at 800 °C for 6 h. Chemical purity of the samples was confirmed by powder XRD (PANalytical XRD machine with CuKα radiation). Formation temperature of the spinels were ascertained

* Corresponding author. Tel.: +91 4565 227559x243; fax: +91 4565 227779.
E-mail address: raguphysica@yahoo.co.in (K. Ragavendran).

0921-4526/$ - see front matter © 2009 Elsevier B.V. All rights reserved.
doi:10.1016/j.physb.2009.04.019

using Polymer Laboratories (UK) STA 1500 thermal analyzer. Information on the oxidation states of manganese is obtained using Thermo Fischer (UK) multi-lab 2000 X-ray photoelectron spectrometer (MgKα radiation) fitted with a twin anode X-ray source. Morphology of the materials are recorded using a Hitachi, model S3000 H, scanning electron microscope.

A crystal shape algorithm is used to generate the crystal habits and the nature of the exposed *hkl* planes of the cathode materials under investigation from the 2θ values and FWHM of their respective XRD peaks. The atomic arrangement on the exposed *hkl* plane, which will determine a host of electrochemical properties, is obtained by cleaving the $LiMn_2O_4$ crystal along the *hkl* planes of interest, to a depth of 2A°, using the quantum ab inito software CASTEP [17]. All the computations were run on a 2.80 GHz Pentium-IV processor.

3. Results and discussion

3.1. Lattice contraction

The X-ray diffraction patterns of the two batches of $LiMn_2O_4$ are shown in Fig. 1 and the peak positions of the different *hkl* planes are presented in Table 1. It is interesting to see that in the PVA assisted case, there is a consistent increase in the 2θ values for all the *hkl* planes as compared to that for the starch assisted compound, which according to Bragg's equation would imply a lattice contraction in $LiMn_2O_4$(P).

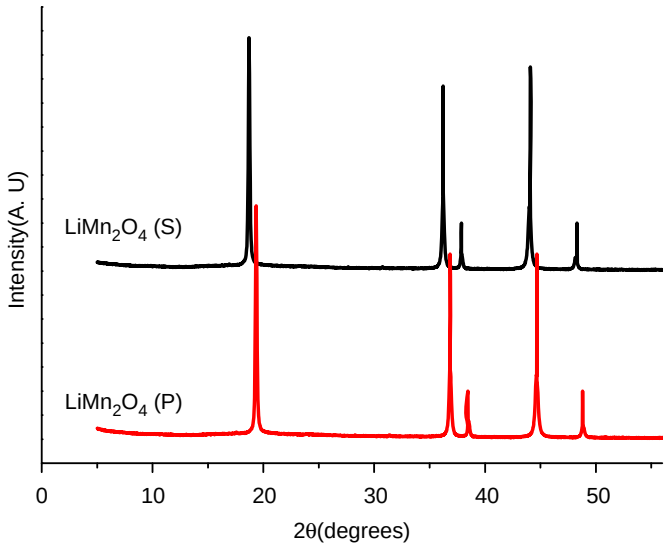

Fig. 1. XRD of $LiMn_2O_4$(S) and $LiMn_2O_4$(P): the latter shows a shift in the 2θ values to the right indicating a lattice contraction.

Table 1
Shift in the 2θ values observed in the X-ray diffraction pattern of lithium manganate prepared through the starch assisted route ($LiMn_2O_4$(S)) and the PVA assisted route ($LiMn_2O_4$(P)) for the various *hkl* planes.

hkl directions	2θ values from X-ray diffraction pattern	
	$LiMn_2O_4$(S)	$LiMn_2O_4$(P)
111	18.70	19.34
311	36.28	36.90
222	37.94	38.56
400	44.08	44.70
331	48.28	48.90
511	58.38	58.90

Thermo gravimetric and differential thermal analysis results on $LiMn_2O_4$(S) and $LiMn_2O_4$(P) are shown in Figs. 2a and b, respectively. It can be seen from these figures that the spinel formed by PVA assisted route has a larger formation temperature (515 °C) compared to that formed by the starch (490.23 °C) assisted route.

It is immediately not obvious as to why $LiMn_2O_4$(P) should have a higher formation temperature compared to $LiMn_2O_4$(S). It can be seen from Fig. 2 that the slope of the TG curve for $LiMn_2O_4$(P) is sharp compared to that for $LiMn_2O_4$(S). Also, the DTA curve for the former has recorded a single peak while that in the latter shows at least two shoulders in addition. These observations may most likely be attributed to the formation of some intermediates when using starch as the fuel, which consequently brings down the formation temperature. Further work is required to understand this mechanism. It is likely that the higher formation temperature for the spinel formed under PVA assistance leads to an internal heating of the material, favoring the oxidation of a fraction of Mn^{+3} (ionic radius: 0.65 Å) to Mn^{+4} with a lower ionic radius (ionic radius: 0.53 Å) leading to a lattice contraction.

XPS measurements on $LiMn_2O_4$(S) and $LiMn_2O_4$(P) are presented in Fig. 3. Chowdari et al. reported that the $Mn2p_{3/2}$ binding energy (BE) of Mn^{3+} and Mn^{4+} are located at 641.9 and 643.2 eV, respectively [18]. In our case, the $Mn2p_{3/2}$ BE of $LiMn_2O_4$(S) and $LiMn_2O_4$(P) are, respectively, at 642.15 and 642.73 eV, indicating that the manganese valence states in our compounds is a mixture of +3 and +4, with $LiMn_2O_4$(P) containing slightly a larger fraction of Mn^{4+} content than $LiMn_2O_4$(S). The higher content of Mn^{4+} in $LiMn_2O_4$(P), as confirmed by XPS, provides a satisfactory explanation for lattice contraction in this material.

It is interesting to mention an earlier report which has made a similar observation on the shift in the 2θ to the higher values in the XRD pattern of $La_{0.53}Tb_{0.14}Sr_{0.33}MnO_{3\pm\delta}$ sintered under different atmospheres [9]. These authors attribute the shift to a variation in the oxygen stoichiometry and hence to a change in the Mn^{3+}/Mn^{4+} ratio in the compounds prepared under different sintering conditions. It is important to note that the 2θ shift observed by these authors is not as large as that reported by us (~0.6° shift towards the right for all the *hkl* peaks) for lithium manganate. This huge shift in the 2θ to the right indicates a lattice contraction in $LiMn_2O_4$(P) compared to $LiMn_2O_4$(S). (A detailed X-ray crystallographic study of these materials is under progress.)

Thus, the shift in the 2θ values in $LiMn_2O_4$(P) cannot be explained as solely due to an increase in the Mn^{4+} fraction. A satisfactory conjecture would be that PVA somehow increases the compressibility of $LiMn_2O_4$ so that even a small change in the Mn^{3+}/Mn^{4+} ratio manifests itself as a huge variation in the lattice parameter of the material, thus causing the observed shift in the 2θ. It is pertinent to mention here that Yamaura et al. have reported on the application of lithium manganate as a prototype material in the study of high pressure phase transitions in Earth's mantle [8]. They have reported that $LiMn_2O_4$ undergoes the spinel to calcium ferrite type transition at a much moderate pressure range of 6 GPa compared to ~25 GPa needed to observe this transition in $MgAl_2O_4$ [19]. It is most likely that a higher compressibility intrinsic to $LiMn_2O_4$ allows for such phase transitions at relatively low pressures.

If it is proved that $LiMn_2O_4$ prepared through the PVA route enhances the compressibility even more, then it would be a contribution to the area of 'high pressure mineral physics' [20,21] to mimic the Earth's lower mantle with relatively much lower experimentally achievable pressures.

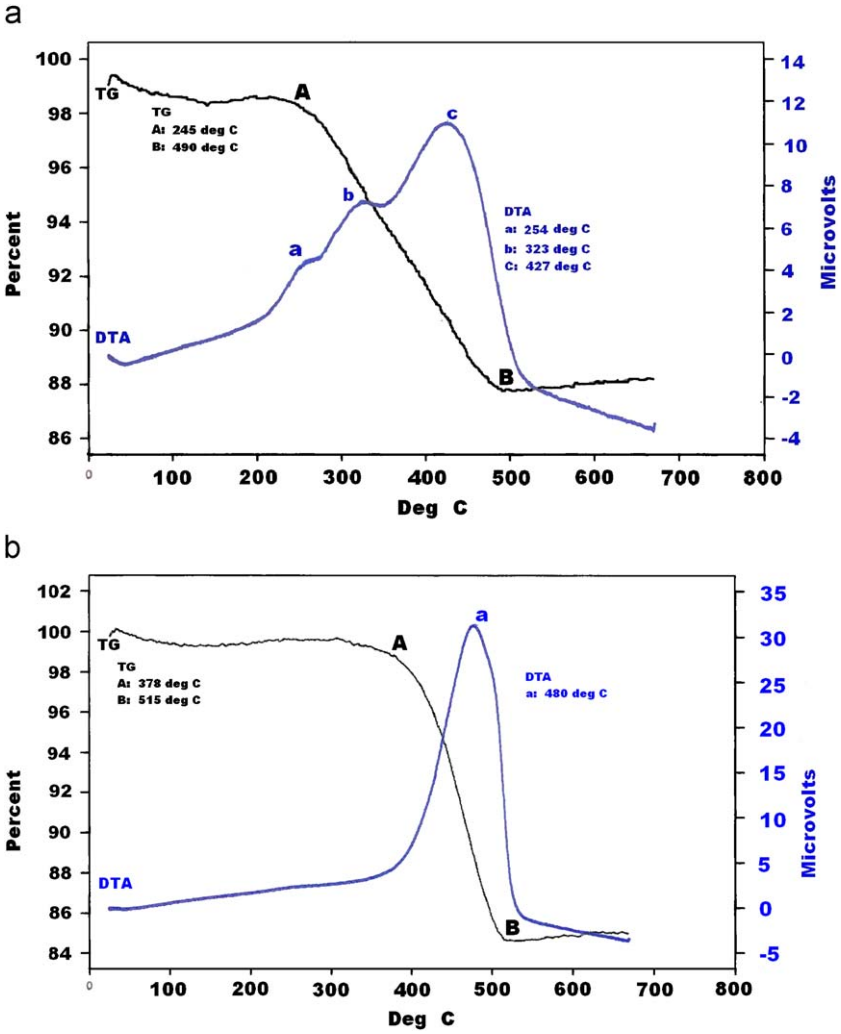

Fig. 2. (a) TG/DTA for $LiMn_2O_4$(S). (b) TG/DTA for $LiMn_2O_4$(P).

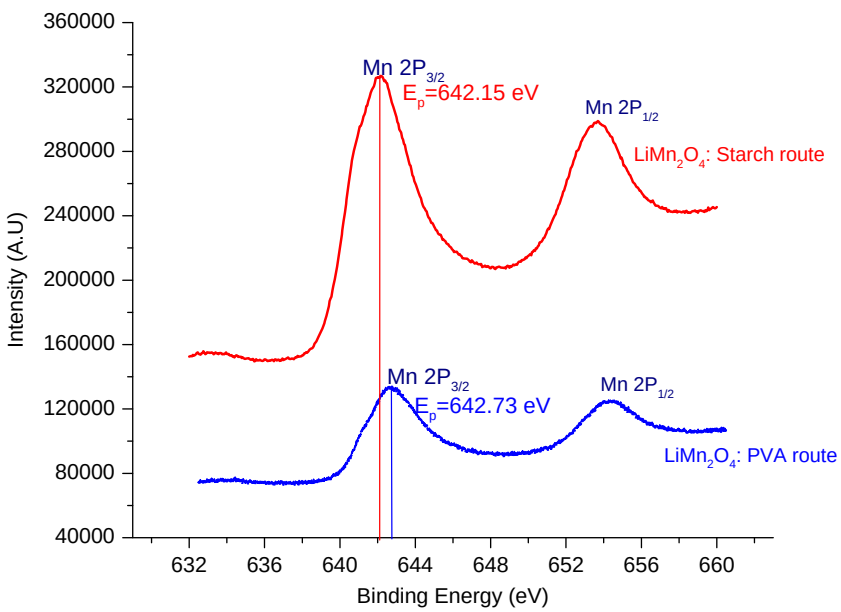

Fig. 3. $Mn2p_{3/2}$ XPS scan on $LiMn_2O_4$(S) and $LiMn_2O_4$(P).

3.2. Crystal habits of lithium manganate and prediction of their electrochemical properties

The structure and morphology of lithium manganate will have a profound impact on the electrochemical properties. Morphology dependent electrochemical properties of $LiMn_2O_4$ are recently reported in the literature [22–24]. In these reports the electrochemical properties are correlated with the peak intensities of the *hkl* planes obtained from XRD. However, XRD can only capture the internal crystal structure of a material while the morphology dependent electrochemical properties arise out of the external crystal shape (also known as the crystal habit). While SEM/TEM can provide visual photograph of the crystal, assigning a unique miller index (h k l) to each of the crystal faces exposed is not straight forward. It is pertinent to mention here that experimental techniques such as the low energy electron diffraction (LEED) unlike XRD can deliver direct information on the crystal habit. However, such reports are not available in the literature to the best of our knowledge.

In this section we use a crystal shape algorithm which requires inputs from the XRD of the material such as the 2θ values and the FWHM of the XRD peaks corresponding to different *hkl* planes to generate the crystal shape (habit) and quantitative information on the area of the exposed *hkl* planes.

Fig. 4 shows the crystal shapes of $LiMn_2O_4$(S) and $LiMn_2O_4$(P) as generated by the crystal shape algorithm. SEM images of these two materials are also shown for comparison. It can be seen that PVA assists in the formation of better crystallites compared to starch. Higher crystallinity is known from the literature to improve the stability of the crystallographic structure and electrochemical cyclability of the lithium battery by hindering Mn dissolution [25–27]. In tune with these experimental findings our crystal shape algorithm predicts that the more crystalline $LiMn_2O_4$(P) will be less prone to Mn dissolution compared to $LiMn_2O_4$(S).

Morphology as seen from SEM/TEM should be clearly distinguished from the shape/habits of the underlying crystallites.

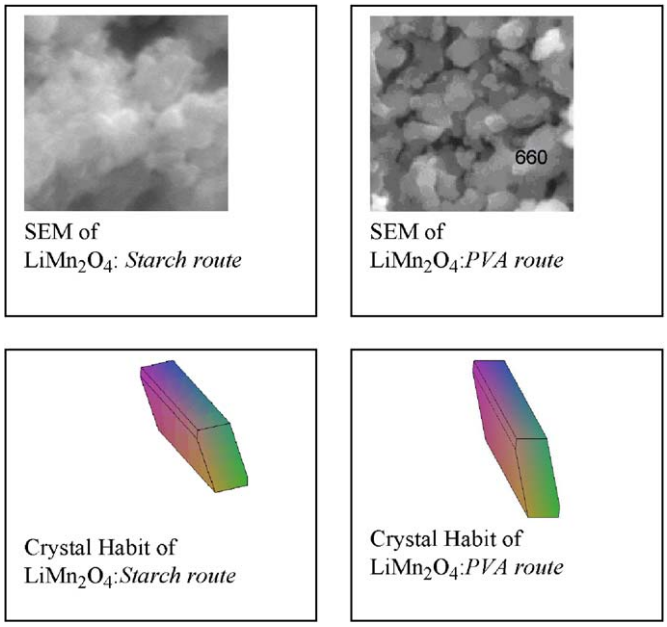

Fig. 4. SEM images and the crystal shapes (as generated by the crystal shape algorithm) of $LiMn_2O_4$ prepared through the starch and PVA assisted routes.

Table 2
Quantitative crystal habit information on $LiMn_2O_4$ prepared through starch and PVA assisted routes.

$LiMn_2O_4$(S)[a]		$LiMn_2O_4$(P)[b]	
Exposed *hkl* plane (area in Å^2)	Unexposed planes	Exposed *hkl* plane (area in Å^2)	Unexposed planes
111 (96533)	222	111 (26492)	222
311 (20206)	511	311 (5451)	511
400 (88422)		400 (23260)	
331 (187168)		331 (48726)	

[a] Starch assisted combustion method.
[b] PVA assisted combustion method.

While the shape/habit is a property which depends upon the individual crystallite, the morphology is a result of an agglomeration of a large number of crystallites. Therefore there need not be a one to one correspondence between the morphology and the underlying crystal habits. Though the crystal shape of the individual crystallites, as generated by the algorithm, of $LiMn_2O_4$(S) is almost the same as that of $LiMn_2O_4$(P) it can be seen from Table 2 that a decrease in the area of all the crystallographic planes is observed when PVA is used as the fuel. The atomic arrangement on the various *hkl* planes of $LiMn_2O_4$ obtained using CASTEP is shown in Fig. 5a (Mn atoms buried inside the *hkl* planes) and Fig. 5b (Mn atoms located on the surface of the *hkl* planes).

Minimal exposure in $LiMn_2O_4$(P) of the [3 3 1] plane which contains Mn atom on the plane indicates that this material is less prone to Mn dissolution and hence would possess a higher cycle life compared to $LiMn_2O_4$(S). Though all the exposed *hkl* planes in these two materials contain the same number of 8a sites that could intercalate Li atoms, the area of all the *hkl* planes is consistently smaller in $LiMn_2O_4$(P). In general, it can be concluded that while lithium manganate prepared through the PVA assisted route would deliver a higher cycle life, that prepared through starch route would render the battery with a higher rate capability.

4. Conclusions

Lattice parameter of a crystal and the charge state on the atoms constituting the crystal lattice are among the foremost attributes that decide the physics and electrochemistry of a material. In the present work we report an interesting observation on a huge lattice contraction in $LiMn_2O_4$ depending on the fuel used for the preparation. XRD data clearly show that $LiMn_2O_4$ prepared by PVA route has undergone a huge lattice contraction as compared to that prepared by starch route. The higher formation temperature for $LiMn_2O_4$(P) is believed to convert some of the Mn^{3+} to Mn^{4+} with a smaller ionic radius. This is in fact confirmed through XPS studies which indicate the presence of a larger fraction of Mn^{4+} in $LiMn_2O_4$(P) accounting for the observed lattice contraction in this material. Our crystal shape algorithm predicts that $LiMn_2O_4$(P) is less prone to Mn dissolution and hence would deliver a higher electrochemical cyclability compared to $LiMn_2O_4$(S).

Our future work will focus on a detailed experimental study on the electrochemistry and physics of these materials. Lithium cells will be assembled using these materials and the predictions of the crystal shape algorithm will be verified.

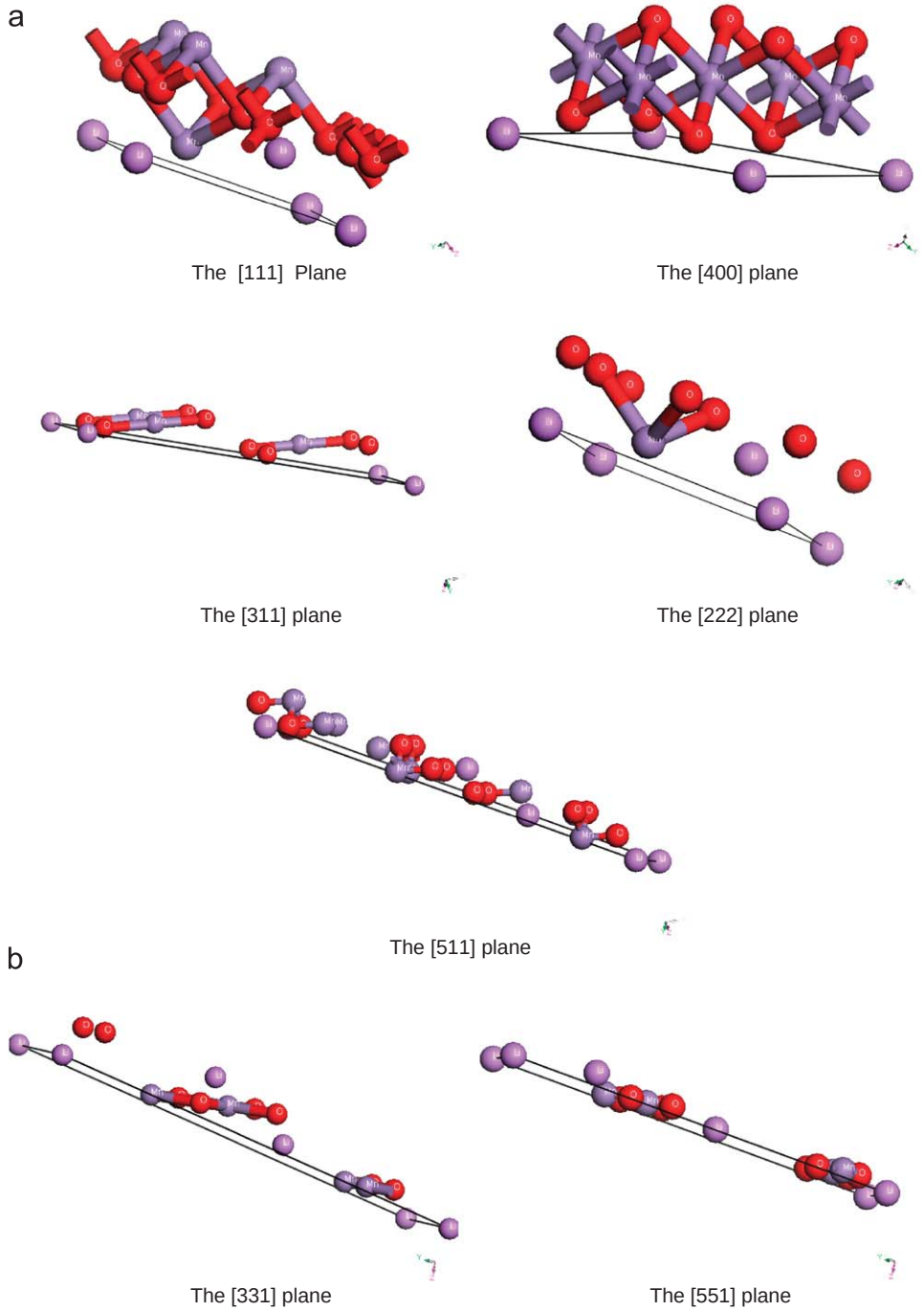

Fig. 5. (a) Atomic arrangement of Mn atoms on different planes (Mn atoms are buried inside the *h k l* planes). (b) Atomic arrangement of Mn atoms on different *h k l* planes (Mn atoms are located on the *h k l* planes). Note: Li, Mn and O are marked with light purple, dark purple and red spheres, respectively, each sphere carrying the symbol of the element it represents (for interpretation of the references to color in this figure legend, the reader is referred to the web version of this article).

Acknowledgments

This work was partly supported by the Department of Science and Technology (government of India, New Delhi) through a project (GAP 39/05) on lithium batteries. One of the authors (K.R.) thanks the CSIR, government of India for the award of an Extended Senior Research Fellowship. K.R. is grateful to Dr. A. Veluchamy of CECRI for providing support for his Ph.D. work at CECRI. The authors also thank Mr. Prasath of I.I.Sc. Bangalore, India and Dr. H.L. Chou of NTUST, Taipei, Taiwan for useful discussions on the use of CASTEP. We also thank an anonymous reviewer for his valuable comments.

References

[1] M. Wakihara, G. Li, H. Ikuta, in: M. Wakihara, O. Yamamoto (Eds.), Lithium Ion Batteries (Fundamentals and Performance), Wiley-VCH, New York, 1998.
[2] H.M. Wu, J.P. Tu, Y.F. Yuan, Y. Li, W.K. Zhang, H. Huang, Physica B 369 (2005) 221.
[3] J. Tu, X.B. Zhao, D.G. Zhuang, G.S. Cao, T.J. Zhu, J.P. Tu, Physica B 382 (2006) 129.
[4] K. Ragavendran, D. Vasudevan, A. Veluchamy, B. Emmanuel, J. Phys. Chem. B 108 (2004) 16899.
[5] D. Sherwood, K. Ragavendran, B. Emmanuel, J. Phys. Chem. B 109 (2005) 12791.
[6] R. Carvajal, G. Rousse, C. Masquelies, M. Hervieu, Phys. Rev. Lett. 81 (1998) 4660.
[7] R. Basu, C. Felner, A. Maignan, R. Seshadri, J. Mater. Chem. 10 (2000) 1921.

[8] K. Yamaura, Q. Huang, L. Zhang, K. Takada, Y. Baba, T. Nagai, Y. Matsui, K. Kosuda, E.T. Muromachi, J. Amer. Chem. Soc. 128 (2006) 9448.
[9] E.P. Rivas-Padilla, W.A. Ortiz, J. Magn. Magn. Mater. 279 (2004) 51.
[10] C. Kapusta, P.C. Riedi, J. Magn. Magn. Mater. 196–197 (1999) 446.
[11] D. Groult, C. Martin, A. Maignan, D. Pelloquin, B. Raveau, Solid State Commun. 105 (1998) 583.
[12] P. Strobel, A. Ibarra Palos, M. Anne, F. Le Cras, J. Mater. Chem. 10 (2000) 429.
[13] Y.S. Horn, R.L. Middaugh, Solid State Ionics 139 (2001) 13.
[14] P. Kalyani, N. Kalaiselvi, N. Muniyandi, J. Power Sources 11 (2002) 232.
[15] K. Ragavendran, V. Morchshakov, A. Veluchamy, K. Bärner, J. Phys. Chem. Solids 69 (2008) 182.
[16] D. Sherwood, B. Emmanuel, Cryst. Growth Design 6 (2006) 1415.
[17] M.D. Segall, et al., J. Phys. Condens. Matter 14 (2002) 2717.
[18] K.M. Shaju, G.V. Subba Rao, B.V.R. Chowdari, Solid State Ionics 152–153 (2002) 69.
[19] K. Yamaura, Q. Huang, L. Zhang, K. Takada, Y. Baba, T. Nagai, Y. Matsui, K. Kosuda, E. Takayama-Muromachi, Phys. Stat. Sol. (b) 244 (2007) 285.
[20] P.W. Bridgman, Nobel Lectures in Physics, 1946.
[21] J. Chen, Y. Wang, T.S. Duffy, G. Shen, L.F. Dobrzhinetskaya (Eds.), Advances in High-pressure Techniques for Geo-physical Applications, Elsevier, Amsterdam, ISBN 978-0-444-51979-5, 2005.
[22] H.-L. Zhu, Z.-Y. Chen, S. Ji, V. Linkov, Solid State Ionics 179 (2008) 1788.
[23] D. Kyung Kim, et al., Nano Letters 8 (2008) 3948.
[24] J.Y. Luo, H.M. Xiong, Y.Y. Xia, J. Phys. Chem. C 112 (2008) 12051.
[25] A. Blyr, C. Sigala, G. Amatucci, D. Guyomard, Y. Chabre, J.M. Tarascon, J. Electrochem. Soc. 145 (1998) 194.
[26] Y. Gao, J.R. Dahn, J. Electrochem. Soc. 143 (1996) 100.
[27] K. Kanamura, K. Dokko, T. Kaizawa, J. Electrochem. Soc. 152 (2005) A391.